# Simulation of interlayer coupling for electroactive covalent organic framework design

Tanner M. Leo, $^{\dagger,\parallel}$  Megan Robbins, $^{\ddagger,\parallel}$  Alana Sullivan, $^{\dagger,\parallel}$  Henry Thornes, $^{\ddagger}$  Garrett Fitzsimmons, $^{\dagger}$  Alyssa Goodey, $^{\P}$  and Tim Kowalczyk $^{*,\S}$ 

†Advanced Materials Science & Engineering Center, Western Washington University,
Bellingham, WA 98225, USA

‡Department of Chemistry and Advanced Materials Science & Engineering Center,
Western Washington University, Bellingham, WA 98225, USA

¶Department of Chemistry and Institute for Energy Studies, Western Washington
University, Bellingham, WA 98225, USA

§Department of Chemistry, Advanced Materials Science & Engineering Center, and
Institute for Energy Studies, Western Washington University, Bellingham, WA 98225, USA

|| These authors contributed equally to this work.

E-mail: Tim.Kowalczyk@wwu.edu

#### Abstract

Porous, stacked two-dimensional covalent organic frameworks (2D COFs) bearing semiconducting linkers can support directional charge transfer across adjacent layers of the COF. To better inform current and possible future design rules for enhancing electron and hole transport in such materials, an understanding of how linker selection and functionalization affects interlayer electronic couplings is essential. We report electronic structure simulation and analysis of electronic couplings across adjacent linker units as well as to encapsulated species in functionalized electroactive 2D COFs. The detailed dependence of these electronic couplings on interlayer interactions are examined through scans along key interlayer degrees of freedom and through configurational sampling from equilibrium molecular dynamics on semiempirical potential energy surfaces. Beyond affirming the sensitivity of the electronic coupling to interlayer distance and orientation, these studies offer guidance toward linker functionalization strategies for enhancing charge carrier transport in electroactive 2D COFs.

#### 1 Introduction

The molecular design space afforded by the discovery and development of covalent organic frameworks (COFs) is large and continues to expand rapidly. <sup>1–3</sup> While porosity drives the majority of scientific, industrial, and commercial interest in COFs, <sup>4,5</sup> the ability to embed and encapsulate photophysically or electrochemically active species in 2D COFs has led to the development of a variety of photoactive and electroactive COFs. <sup>6,7</sup> There is significant interest in their potential applications in sustainable energy including solar cells, <sup>8</sup> photoswitchable conductivity, <sup>9</sup> and electro- and photocatalysis, <sup>10–13</sup> as well as in small-molecule sensing. <sup>14</sup> A number of recent works have elucidated design principles for photoactive and electroactive COFs, including as electrocatalysts, <sup>15,16</sup> as photocatalysts, <sup>17,18</sup> as electrochemiluminescent materials <sup>19</sup> and as electrode materials in Li-ion cells. <sup>20</sup> Side-chain engineering and post-synthetic functionalization can be used to increase the crystallinity of 2D-COFs<sup>21</sup>

and to tune their photophysical properties. <sup>22–24</sup>

The rapid expansion of synthetic strategies for the construction and functionalization of COFs<sup>25,26</sup> allows for a closer feedback loop between synthesis, characterization, and modeling in the design and development COFs with targeted properties.<sup>27,28</sup> As the computational materials science community expands its efforts in high-throughput virtual screening of COFs and related reticular structures for optimizing targeted physical and chemical properties, <sup>29–33</sup> it will become increasingly important for computational models to capture finer details of dynamical COF structure and electronic interactions that, while crucial for materials performance, are often overlooked due to the computational cost associated with quantum chemical modeling of such large systems.

A primary focus for theoretical modeling of electroactive COFs, as with other organic semiconductors,  $^{34,35}$  is charge carrier mobility analysis.  $^{36,37}$  While band-like transport within or across layers is observed experimentally  $^{38,39}$  and predicted theoretically  $^{40}$  in certain COFs, a charge hopping model is a suitable starting point when the charge carrier is relatively localized to one layer. Such hopping models are rooted in the Marcus theory of electron transfer, an approach that requires knowledge – typically from quantum chemical calculations – of the driving force  $\Delta G$  (if the initial and final state are nondegenerate), the reorganization energy  $\lambda$ , and the electronic coupling V which together determine the charge transfer (CT) rate,

$$k_{\rm CT} = \frac{2\pi}{\hbar} \frac{V^2}{\sqrt{4\pi\lambda k_{\rm B}T}} \exp\left[-\frac{(\lambda + \Delta G)^2}{4\lambda k_{\rm B}T}\right]$$

While all of these properties are crucial to proper first-principles modeling of the mobility, the electronic couplings stand out due to their high sensitivity to interlayer proximity and orientation. They are also arguably more difficult to compute because they are a transition property, i.e. a property of both the initial and final electronic states involved in the process. Approaches for the evaluation of these electronic couplings include the generalized Mulliken-Hush method, <sup>41–43</sup> multi-state density functional theory (DFT) and constrained DFT-based configuration interaction (CDFT-CI), <sup>44–46</sup> transition density-based approaches, <sup>47</sup> and the

dimer projection method. 48

In this work, we address three distinct but thematically interrelated questions about how linker functionalization in COFs influences their electroactivity through a combination of semi-empirical molecular dynamics (MD) and density functional theory (DFT) calculations. First, we ask how functionalization of planar 2D COFs by small functional groups with an asymmetrically out-of-plane component affects interlayer stacking in the COF and, therefore, interlayer electronic couplings for electron and hole mobility in the material. Second, we examine how the arrangement of linker functionalization from one layer to the next influences orientational sensitivity of the electronic coupling. Finally, we consider how electronic coupling between a COF and an encapsulated species is influenced by interlayer stacking in the COF. We conclude with some unifying observations and reflections on their implications for electroactive COF design.

# 2 Computational Details

All COF structures in this study were prepared through modification of existing optimized COF models as follows; abbreviated names for each system are introduced in Sec. 3 but adopted here in advance for brevity. The MTP-COF model was constructed via functionalization of a pentacene-based COF model previously prepared by us, <sup>49</sup> while the TBP-COF model was constructed from a closely related structure reported recently. <sup>38</sup> Modeling of PD-COF layers was only performed on fragments, so crystal structures of the full COF unit cells were not required. The PCBM@TT-COF model was developed by combining a geometry-optimized structure of an isolated PCBM molecule with the reported powder X-ray diffraction (PXRD)-derived structure of TT-COF. <sup>50</sup> For MTP-COF and TBP-COF, initial structures and unit cells were optimized in DFTB with the matsci Slater-Koster parameter set <sup>51,52</sup> under periodic boundary conditions, including reoptimization of lattice vectors. All DFTB calculations reported in this work were performed with the DFTB+ package <sup>53</sup> v.20

or higher. For PCBM@TT-COF, the large size of the encapsulated PCBM would require more TT-COF layers than we could include in the CDFT-CI electronic coupling analysis. Therefore, we generated single-, double-, and triple-layer TT-COF models without periodic boundary conditions and embedded the PCBM at the center of the structure for analysis of electronic couplings as a function of displacement along the pore axis.

For thermal configurational sampling of MTP-COF and TBP-COF, electronic couplings for electron transfer, hole transfer, and charge transfer excitation were evaluated at 250 snapshots extracted from DFTB MD. Production MD was performed on pre-equilibrated structures in the NVT ensemble at  $T=300~\rm K$  with configurations sampled every 20 timesteps (every 10 fs). For each snapshot, a pair of adjacent linker fragments, together with their boronate ester linkages, were extracted from the full COF structure and hydrogen-capped. A constrained geometry optimization at the PBE/3-21G level<sup>54</sup> allowed for relaxation of the introduced hydrogens' positions while holding the rest of the extracted structures frozen. Electronic couplings between the layers were then computed using the constrained DFT configuration interaction (CDFT-CI) approach  $^{45,46}$  at the PBE/6-311G\* level.

Electronic couplings for the PD-COF fragments were computed at fixed, constrained geometries as described in Sec. 3.2 using CDFT-CI at the B3LYP/6-311G\* level. <sup>55</sup> PCBM@TT-COF couplings were also computed with the B3LYP functional, but the large system size necessitated use of a more minimalistic 3-21G basis set. All DFT calculations reported in this work were performed with the Q-Chem 5.0 package. <sup>56</sup>

## 3 Results and Discussion

#### 3.1 Interlayer stacking analysis of nonplanar linkers

Functionalization of 2D COFs with nonplanar linkers offers a degree of control over interlayer spacing and orientation. However, the precise impact of a chosen functional group on the interlayer stacking, and therefore on the electronic coupling across layers, is complicated by

the potential for conformational flexibility of the introduced functional group, which may then be amplified any flexibility of the framework itself.<sup>49</sup>

To determine how nonplanar linker substitution affects the electronic couplings governing charge carrier migration across layers in substituted 2D COFs, we studied the two COFs depicted in Fig. 1 with acene-like linkers. The 6,13-bis(methylthio)pentacene (MTP)<sup>57</sup> COF forms hexagonal pores via boronate ester linkages to triphenylbenzene spacers (also called cores). The *tert*-butylpyrene (TBP) COF forms square pores via pyrazine linkages to phthalocyanine cores and is the free-base analog of the metal phthalocyanine-based COFs reported by Wang *et al.* <sup>58</sup> The pyrene-pyrazine linkages in TBP-COF form relatively rigid, conjugated azaacene-like structures which constrast with the more flexible, single-bond character of the boronate ester linkage between MTP and triphenylbenzene in MTP-COF.

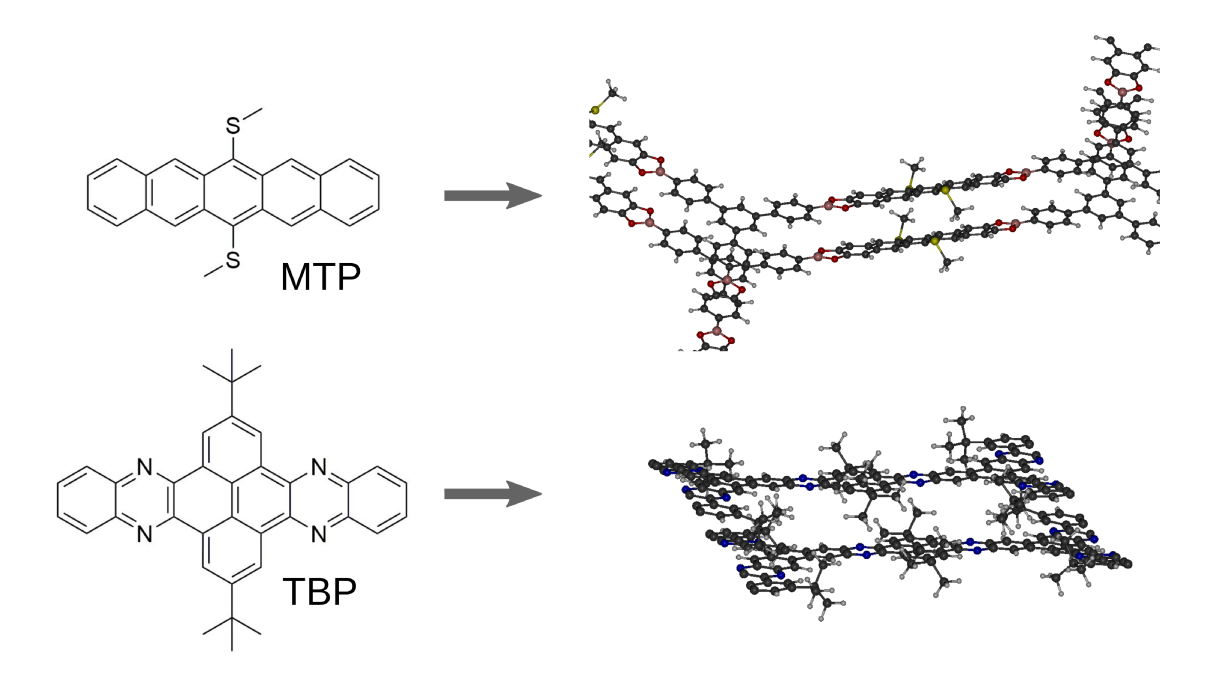


Figure 1: Linker skeletal structures and rendering of a representative bilayer structure of the corresponding 2D COFs. Top: triphenylbenzene boronate ester-linked methylthiopentacene (MTP) COF with hexagonal pores. Bottom: pyrazine-linked t-butylpyrene (TBP) based COF with square pores.

At room temperature, dynamical fluctuations of COF layers lead to a distribution of

interlayer orientations that in turn produce a distribution of interlayer electronic couplings. Here we focus on the angle  $\theta$  between the planes of the adjacent COF linkers as a single-parameter measure of the fluctuating orientations. This angle is illustrated schematically in Fig. 2, where it is labeled the interlayer plane angle.

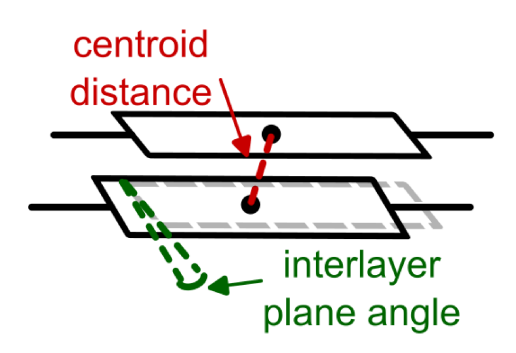


Figure 2: Schematic illustration of key geometric features of stacked COF linkers, represented as black solid rectangles and rotated out-of-plane such that their projections appear as parallelograms: (red dashed line) distance between the centroids of adjacent COF linkers; (angle between green dashed lines) interlayer angle between the planes of adjacent COF linkers. The light grey dashed box is a vertically translated copy of the upper COF linker to guide the eye and clarify the interlayer plane angle measurement.

Histograms illustrating the distribution of  $\theta$  observed over a sample of 250 snapshots from DFTB MD simulations of each COF are depicted in Fig. 3(a) and (d). While the two distributions share a mode at  $\theta = 3^{\circ}$ , the histograms also show the anticipated narrower distribution of interplanar angles for TBP-COF relative to MTP-COF. Importantly, the interplanar angle distribution of MTP-COF is also more skewed, with a tail extending to fluctuations significantly larger than the mode.

If the electronic coupling for charge transport across the layers differs significantly at these extended angles relative to the nearly planar configurations, these differences should manifest in the distribution of electronic couplings, and subsequently in the real-world performance of the material. The distributions of electronic couplings for electron transfer in MTP-COF and TBP-COF, shown in Fig. 3(b) and (e), respectively, reflect this expectation: the skew in the distribution of interplanar angles for MTP-COF corresponds to a right-skewed distribution of electronic couplings for MTP-COF. The distribution of electronic couplings for TBP-COF

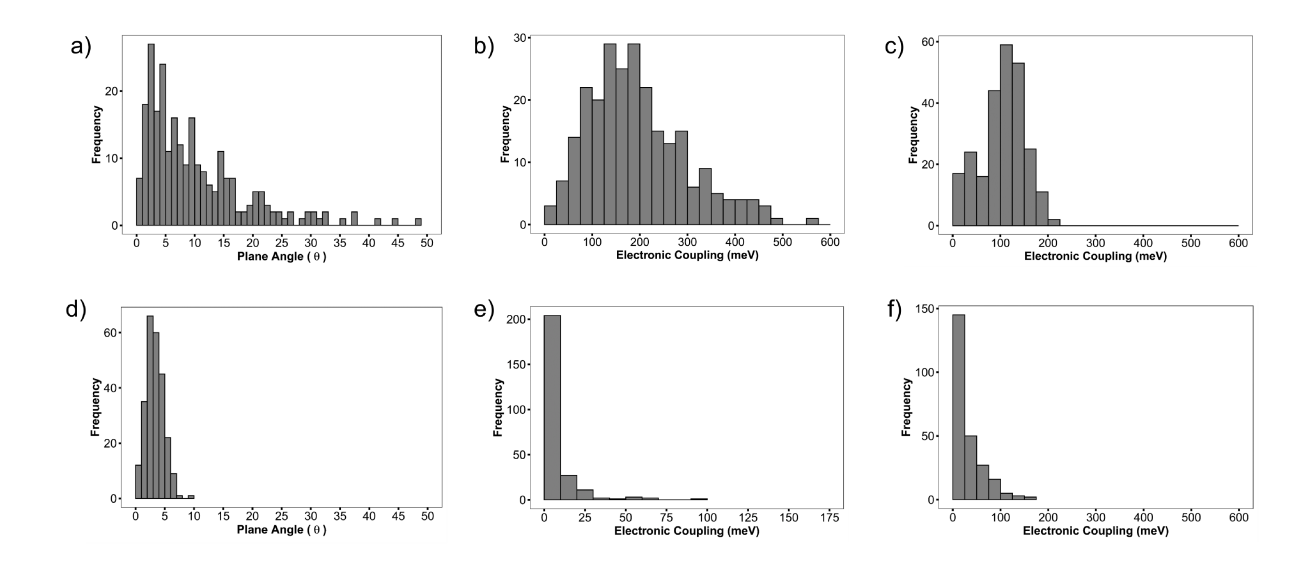


Figure 3: Distribution of inter-chromophore plane angles sampled from MD simulation of (a) MTP-COF and (d) TBP-COF; Distribution of electronic couplings for (b) electron transfer in MTP-COF, (c) hole transfer in MTP-COF, (e) electron transfer in TBP-COF, and (f) hole transfer in TBP-COF.

is much narrower than that of MTP-COF, as is anticipated from the narrow distribution of interlayer angles. However, a nonnegligible number of configurations possess electronic couplings for electron transfer well in excess of the mean for TBP-COF, resulting in an even more skewed distribution than observed for MTP-COF.

Similar to the electronic couplings for electron transfer, the electronic couplings for hole transfer in TBP-COF, Fig. 3(f), also show a larger skew than those of MTP-COF, Fig. 3(c). The larger average couplings and wider distributions for both electron and hole transfer in MTP-COF relative to TBP-COF are consistent with the known enhancement of electronic couplings in certain acene molecular crystals<sup>59,60</sup> and supramolecular complexes<sup>61</sup> with relatively large interplanar angles.<sup>59,60</sup>

The preceding interplanar angle analysis represents an average over the interlayer distances observed in the MD trajectories from which the configurations were sampled. To account for the possibility of distance dependence in the relationship between interplanar angle and electronic coupling, we generated scatterplots of the electronic couplings for electron

and hole transfer in MTP-COF (Fig. 4(a-b)) and in TBP-COF (Fig. 4(c-d)) as a function of both the interlayer angle and the distance between the centroids of the two planar fragments. These interlayer angle and centroid distance measurements are illustrated schematically in Fig. 2. Planes of best fit are overlaid on the plots in grey for reference.

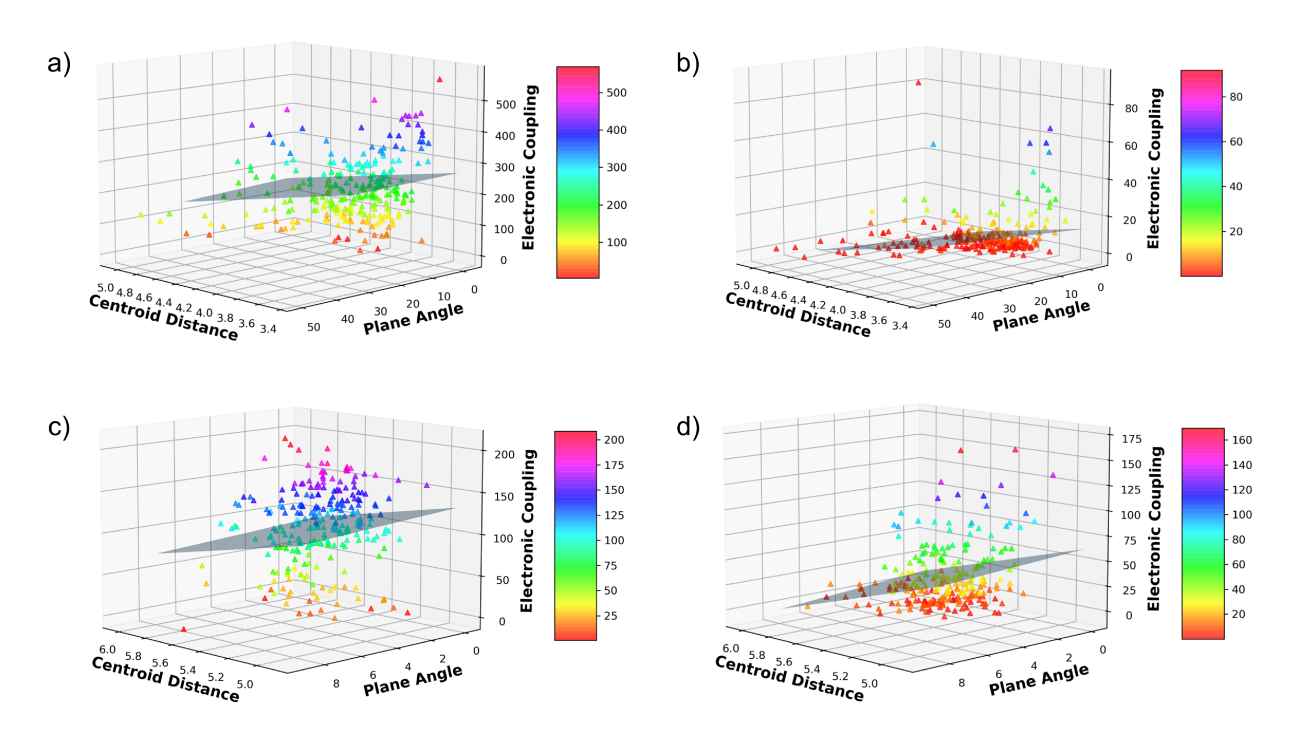


Figure 4: 3D scatterplots illustrating the dependence of electronic coupling on interchromophore distance (Å) and plane angle (°) for configurations sampled from MD simulation of (a) MTP-COF and (d) TBP-COF; Distribution of electronic couplings for (a) electron transfer in MTP-COF, (b) hole transfer in MTP-COF, (c) electron transfer in TBP-COF, and (d) hole transfer in TBP-COF.

Overall, the plots reveal no meaningful interdependence between the interplanar angle and distance in terms of their impact on the electronic couplings. From a design perspective, the independence of these parameters' effects on predicted couplings is a benefit in that it affords independent tunability of the coupling with respect to both parameters, to the extent that they can both be controlled synthetically. 62–64 The larger slope of the best-fit plane with respect to centroid distance, relative to the slope with respect to interlayer angle, in each plot reinforces the expectation that the distance between COF layers is the dominant contributing geometric feature to the electronic coupling, with the interlayer angle playing

an important but secondary role. Specifically, the less bulky —SCH<sub>3</sub> groups on MTP can adopt a staggered orientation across the shorter in-plane axis of the pentacene core in MTP (cf. the 3D model of MTP-COF in Fig. 1) that is unavailable to TBP-COF due to steric crowding of tert-butyl groups across layers. As a result, centroid distances in MTP-COF are roughly 1 Å shorter on average than those of TBP-COF. This shorter distance corresponds to larger electronic couplings on average for electron transfer in MTP-COF than in TBP-COF; in contrast, the more closely packed MTP-COF layers show smaller electronic couplings for hole transfer than TBP-COF. This difference reflects an apparent asymmetry between the coupling strengths for electron and hole transfer between MTP units, with the couplings for hole transfer being markedly smaller on average than for electron transfer.

While our interpretation focuses on the effect of linker functionalization, our calculations cannot exclude the possibility that differences in topology and pore size between the hexagonal MTP-COF and the square TBP-COF also contribute to the observed differences in electronic coupling distributions. A complete disambiguation of these potentially competing factors is beyond the scope of this study but could be accomplished through analogous simulations of COFs in which only the topology or only the linker functionalization is varied.

Altogether, the electronic coupling distributions of these two COFs with nonplanar sidechain-functionalized linkers show that interlayer steric interactions can affect couplings for electron and hole transfer via modulation of both the interlayer spacing and the distribution of interplanar angles observed at room temperature. The lower barrier to interplanar angle rotation for MTP-COF results in more frequent excursions to large interplanar angles, which can enhance the electronic couplings, but also results in greater variability in the coupling relative to more rigid frameworks like TBP-COF.

# 3.2 Parallel and antiparallel interlayer stacking

Asymmetric COF linkers introduce an additional degree of freedom in the 3D stacking of COFs by virtue of how they preferentially orient from one layer to the next. Frey et al. re-

cently reported examples of COFs bearing asymmetric linkers which can give rise to a parallel (P) or antiparallel (AP) arrangement of linkers from one layer to the next. <sup>28</sup> To systematically explore how this asymmetry modulates electronic couplings, we prepared bilayer P and AP configurations of the precursor 4,5-pyrenedione (PD) COF linkers (Fig. 5). We then studied the dependence of electronic couplings for electron/hole transfer, (PD) $^{\pm}$ (PD) $\rightarrow$ (PD)(PD) $^{\pm}$ , and for charge recombination, (PD) $^{+}$ (PD) $^{-} \rightarrow$  (PD)<sub>2</sub>, on two interlayer degrees of freedom: an out-of-plane angle  $\theta$  describing the tilting of one linker relative to the other along the linkers' short axis and defined equivalently to the interplanar angle in Sec. 3.1, and a delamination angle  $\chi$  corresponding to tilting of one linker relative to the other along the long axis of the linker (i.e. along an edge of the COF pores). These angles are also illustrated in Fig. 5.

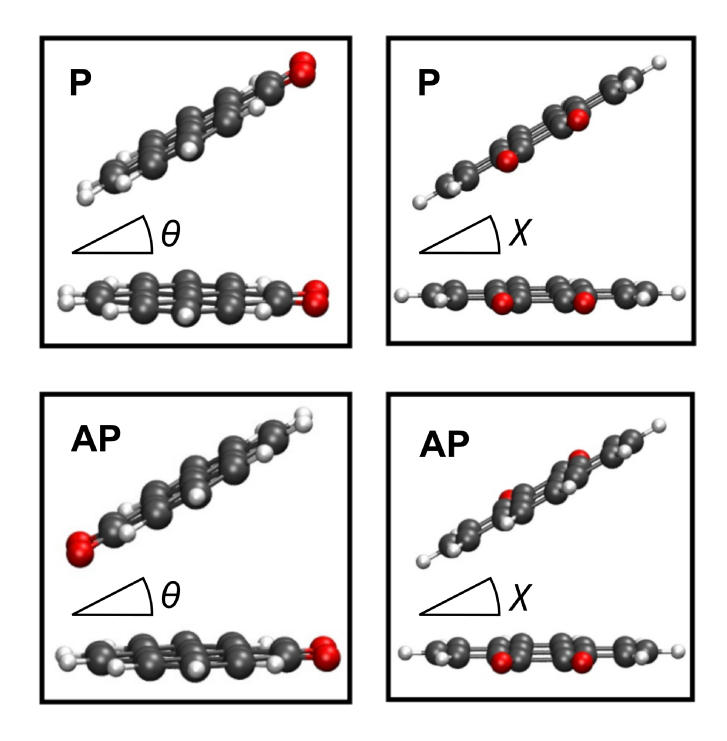


Figure 5: Illustrative orientations of adjacent dione linker fragments studied in this work. Top left: out-of-COF-plane angle  $\theta$ , parallel (P) interlayer orientation. Top right: COF delamination angle  $\chi$ , parallel (P) interlayer orientation. Bottom left: out-of-COF-plane angle  $\theta$ , antiparallel (AP) interlayer orientation. Bottom right: COF delamination angle  $\chi$ , antiparallel (AP) interlayer orientation.

Electronic couplings for electron and hole transfer across PD-COF linkers are shown in

Fig. 6. For the P orientation, both couplings are strongest when the linkers are closest to being co-planar, i.e. at small  $\theta$  and small  $\chi$ . This finding contrasts with the enhancement of electronic coupling for electron and hole transfer in certain acene crystals with a herringbone packing arrangement <sup>60</sup> but is consistent with enhancement of the couplings through stronger  $\pi$ - $\pi$  interaction across the layers. The couplings show the expected exponential decrease with increasing interlayer separation.

Couplings for the AP orientation display a similar decrease with increasing interlayer separation, but the orientation dependence is less straightforward than what we observe for the P orientation. Fig. 6(c) and (g) show an increase in the coupling for electron and hole transfer, respectively, along  $\theta$  out to a second local maximum near 35° for hole transfer and beyond 40° for electron transfer. Along  $\chi$ , a rise in the coupling at larger angles is also visible (Fig. 6(h) and, to a lesser extent, Fig. 6(d)), though it is muted compared to the rise observed along  $\theta$ . Overall, the strongest couplings for electron and hole transfer are achieved in the P orientation at small  $\theta$  and  $\chi$ , while the AP orientation exhibits greater tunability of the coupling with respect to distortions along  $\theta$  and  $\chi$ .

In photoactive COFs, photoexcitation can be harnessed to drive charge separation across layers of the COF.  $^{49,65,66}$  Following the generation of separated charges, the stability of the free charge carriers is subject to the strength of electronic coupling for charge recombination in the COF. In Fig. 7, we show the dependence of electronic couplings for charge recombination across the PD layers on interlayer orientation. The major distinction between the orientation dependence of these couplings and those observed for electron and hole transfer is the clear increase of this coupling with distortion along both  $\theta$  and  $\chi$  for the P orientation. The physical picture that emerges from this analysis is one in which recombination of mobile charge carriers occurs more readily when the P oriented photoactive COF linkers are tilted with respect to one another, whereas electron and hole transfer are more facile when the linker planes are closer to parallel. The picture is less clear when the linkers are in the AP orientation, but all three charge transfer processes appear to possess stronger

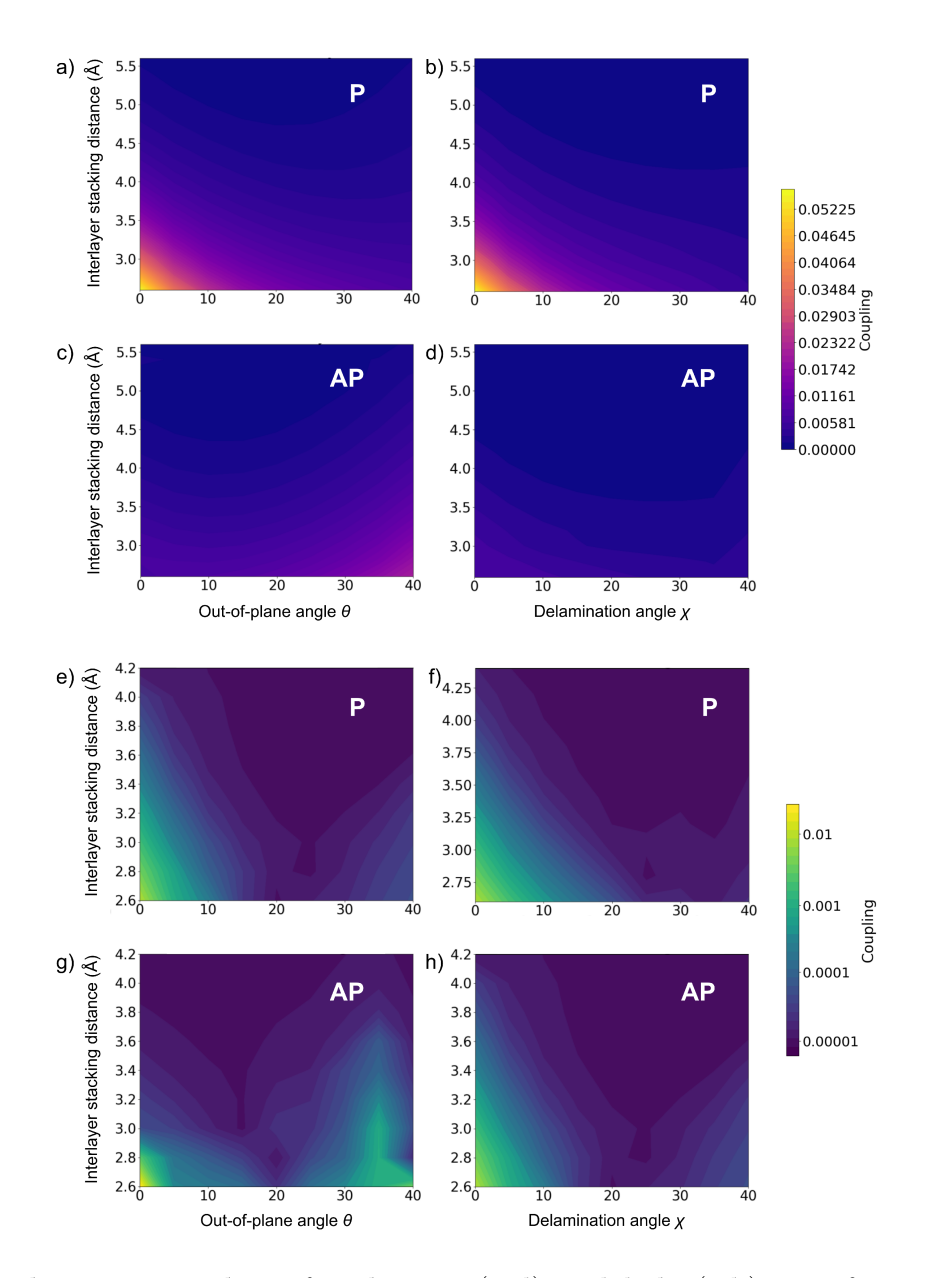


Figure 6: Electronic couplings for electron (a-d) and hole (e-h) transfer across adjacent PD-COF fragments stacked parallel (P) or antiparallel (AP) to one another as a function of interlayer stacking distance and orientational degrees of freedom (cf. Fig. 5). (a,e) P stacking, out-of-plane rotation angle; (b,f) P stacking, delamination angle; (c,g) AP stacking, out-of-plane angle; (d,h) AP stacking, delamination angle. The couplings for hole transfer are plotted logarithmically for ease of interpretation.

couplings at smaller linker distortions for AP-oriented PD-COF. These results suggest that designing photoinduced conformational change into COF linkers could allow for simultaneous enhancement of charge carrier generation and electron/hole transport while suppressing

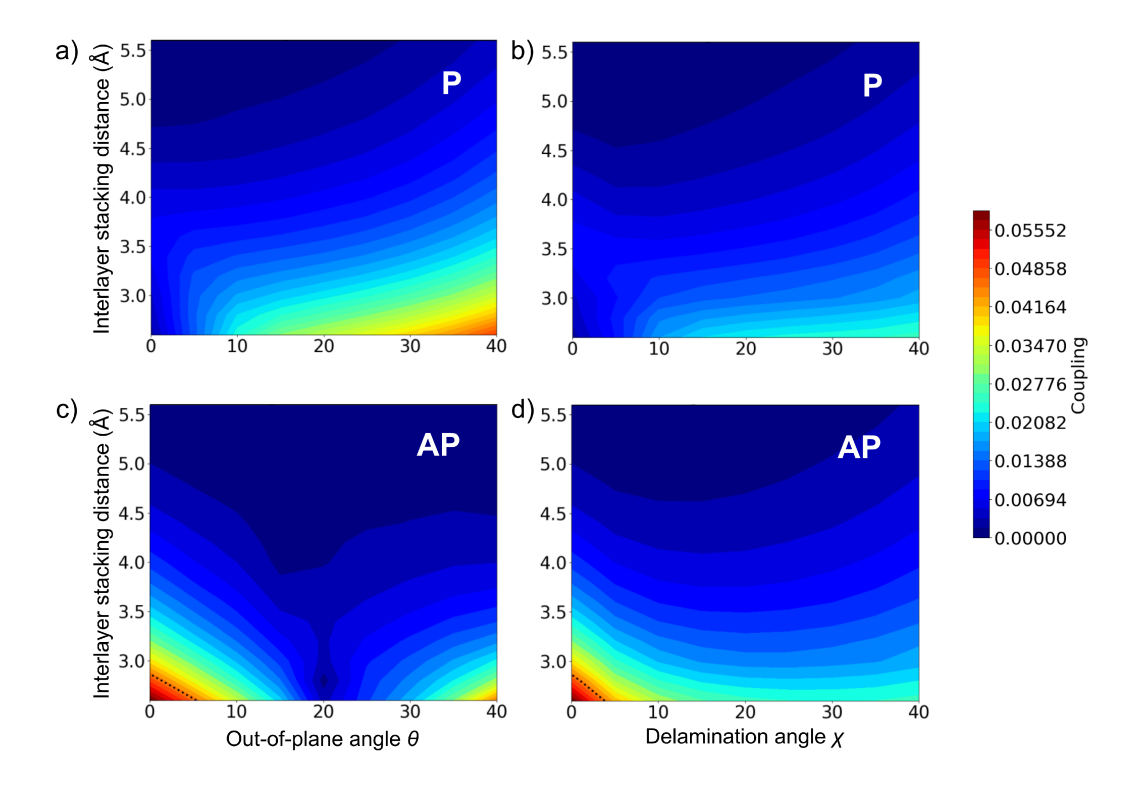


Figure 7: Electronic couplings for charge recombination across adjacent PD-COF fragments stacked parallel (P) or antiparallel (AP) to one another as a function of interlayer stacking distance and orientational degrees of freedom (cf. Fig. 5). (a) P stacking, out-of-plane rotation angle; (b) P stacking, delamination angle; (c) AP stacking, out-of-plane angle; (d) AP stacking, delamination angle.

charge recombination.

### 3.3 Interlayer stacking with encapsulated species

The ability to photoinduce charge separation between the layers of a 2D COF can be combined with the advantage of COF porosity to encapsulate molecular species within the material and generate mobile charge carriers. It has been demonstrated that the encapsulation can drive unique charge separation and recombination kinetics not observed in free solution. <sup>67,68</sup> Here we study how the electronic coupling for electron transfer depends on arrangement of a COF-encapsulated species for a previously reported system consisting of an electroactive thienothiophene (TT)-COF with an encapsulated [6,6]-phenyl-C<sub>61</sub>-butric acid methyl ester (PCBM) fullerene acceptor. <sup>50</sup>

In the PCBM@TT-COF system, PCBM acts as an electron acceptor after photoexcitation of a TT chromophore in TT-COF. Although several electronic couplings connecting different electronic states play a role in the photophysical pathways available to this system, for simplicity we narrow our focus to the electronic coupling for electron transfer from TT-COF to PCBM. We prepared and DFTB-optimized geometries of single-, double-, and triple-layer TT-COF stacks with a single encapsulated PCBM acceptor. We then systematically varied the location of the PCBM along the axis of the pore and evaluated the electronic coupling for electron transfer to PCBM at each position.

Given the high computational cost for obtaining CDFT-CI electronic couplings for a complex of this size, we restrict our analysis to PCBM displacement along the pore axis. Other degrees of freedom such as dependence on distance from PCBM to the pore wall and on interlayer orientation of TT units in the TT-COF wall are also of interest; we aspire to return to them once the semiempirical approach that we are developing for these couplings is implemented and benchmarked. Although we must also resort to a smaller double-zeta basis set for PBCM@TT-COF, we anticipate that trends in the coupling's dependence on geometric parameters will be less sensitive to basis set size and to the degree of exact exchange in the density functional<sup>69</sup> than the absolute magnitude of the coupling itself.

The dependence of the coupling for electron transfer from TT-COF to PCBM on the location of PCBM along the pore axis is shown in Fig. 8 for the single-, double-, and triple-layer TT-COF stacks. The number of TT layers is clearly consequential for the predicted magnitude of the coupling. From this observation, we infer that COF layers beyond the layer closest to the encapsulated species directly impact the strength of the coupling. This dependence can be attributed in part to delocalization of the mobile charge over multiple TT units. Furthermore, the single- and double-layer models exhibit a sloped dependence of the coupling on displacement along the pore axis (best-fit lines in Fig. 8), unlike the triple-layer model for which the electronic coupling is effectively flat along this degree of freedom. The smaller couplings at high vertical displacements that we observe for the triple-layer

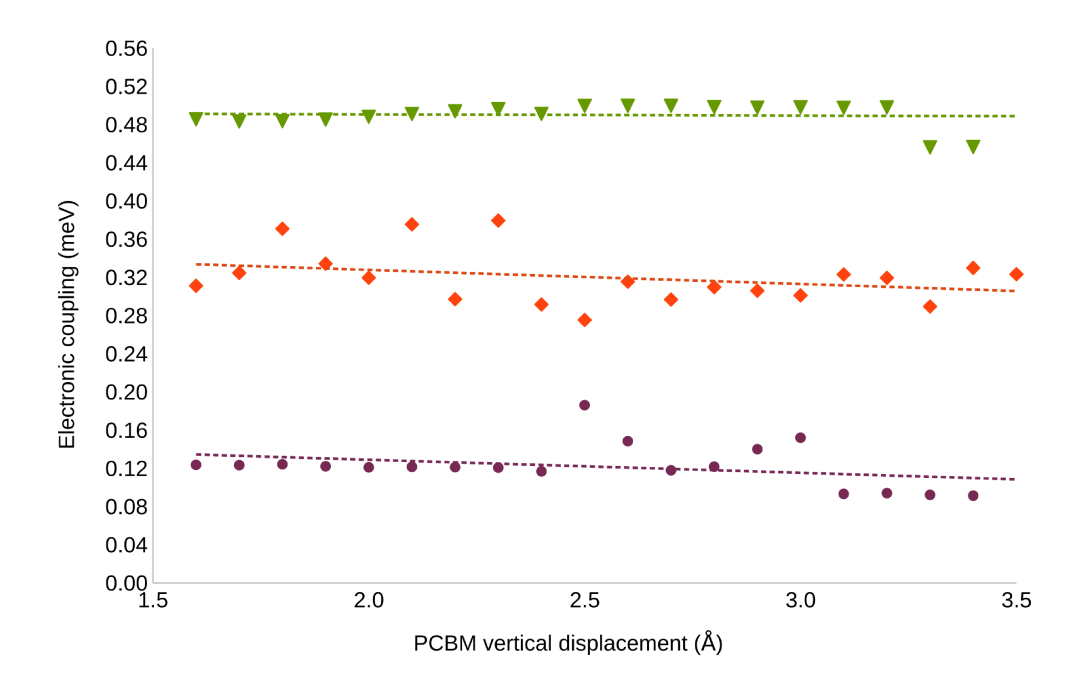


Figure 8: Dependence of the electronic coupling (in meV) for electron transfer from TT-COF to PC<sub>70</sub>BM on displacement (in Å) of PCBM along the axis of the TT-COF pore computed for single-layer (maroon), double-layer (orange), and triple-layer (green) TT-COF models of the full PCCM@TT-COF system.

structure appear to be an artificial edge effect as the PCBM approaches the top of the three-layer stack. This analysis illustrates the importance of including multiple COF layers in the analysis of electronic couplings between COFs and encapsulated species and motivates the development of more approximate models that can accurately compute these couplings over multi-nanometer length scales.

### 4 Conclusion

We simulated the dependence of electronic couplings on orientational degrees of freedom in several classes of electroactive 2D COFs. Functionalization of COFs with nonplanar linkers gives rise to steric interactions that affect the strength of the electronic coupling both through their effect on interlayer spacings and their role in driving fluctuations in the angle between adjacent linkers. We also showed that the arrangement of linker functional groups in parallel

or antiparallel stacks across COF layers can deliver qualitative differences in the dependence of the electronic couplings on interlayer orientation. Finally, the electronic coupling between an electron-donating COF and an encapsulated fullerene acceptor is relatively insensitive to the acceptor's position along the pore axis, but the full triple COF layer encapsulation is necessary to observe this insensitivity in our computational model of the process. These observations, and the methodology we employed to make them, can assist in the articulation of more detailed design rules that should inform development of the next generation of electroactive 2D COFs.

This study builds on our previous findings about the importance of room-temperature configurational sampling of COF orientations<sup>49</sup> by providing examples of how specific orientational features can module electronic couplings in ways that meaningfully affect materials performance. As virtual screening of combinatorially enumerated candidate COF materials becomes more accessible over time, the computational cost of CDFT-CI and other DFT-based means of evaluating electronic couplings for extended COF structures presents a roadblock to meaningful integration of this key information into virtual screenings. Semi-empirical electronic structure methods, such as the DFTB approach used for MD sampling in this work, can be modified to accommodate electronic and spin constraints and thereby obtain electronic couplings for electron/hole transfer and charge separation/recombination much more efficiently than via Kohn-Sham DFT. <sup>70,71</sup> Robust semiempirical evaluation of these electronic couplings would allow for integration of orientation-dependent electronic coupling information into computational screenings and accelerate the development of high-performance COFs for semiconducting, electrochemical, photophysical, and photochemical applications, all of which have a role to play in accelerating the sustinable energy transition.

# 5 Supplementary Material

See Supplementary Material for characterizations of diabatic wavefunction quality for electronic couplings and for reference geometries of COF structures discussed in this work.

# 6 Data Availability Statement

The data that support the findings of this study are available from the corresponding author upon reasonable request.

#### 7 Author Declarations

The authors have no conflicts to disclose.

### 8 Acknowledgments

The authors gratefully acknowledge support from NSF-CAREER award DMR-1848067 and from the Camille and Henry Dreyfus Foundation through a Henry Dreyfus Teacher-Scholar Award (TH-23-014) to TK. The authors thank Zach McGrew for expert support of their use of WWU College of Science and Engineering HPC resources.

#### References

- (1) Evans, A. M.; Strauss, M. J.; Corcos, A. R.; Hirani, Z.; Li, W.; Hamachi, L. S.; Aguilar-Enriquez, X.; Chavez, A. D.; Smith, B. J.; Dichtel, W. R. Two-dimensional polymers and polymerizations. *Chem. Rev.* **2022**, *122*, 442–564.
- (2) Tan, K. T.; Ghosh, S.; Wang, Z.; Wen, F.; Rodríguez-San-Miguel, D.; Feng, J.;

- Huang, N.; Wang, W.; Zamora, F.; Feng, X. et al. Covalent organic frameworks. *Nat. Rev. Methods Primers* **2023**, *3*, 1.
- (3) De Vos, J. S.; Borgmans, S.; Van Der Voort, P.; Rogge, S. M. J.; Van Speybroeck, V. ReDD-COFFEE: a ready-to-use database of covalent organic framework structures and accurate force fields to enable high-throughput screenings. J. Mater. Chem. A 2023, 11, 7468–7487.
- (4) Lohse, M. S.; Bein, T. Covalent organic frameworks: Structures, synthesis, and applications. *Adv. Funct. Mater.* **2018**, *28*, 1705553.
- (5) Li, H.; Dilipkumar, A.; Abubakar, S.; Zhao, D. Covalent organic frameworks for CO<sub>2</sub> capture: From laboratory curiosity to industry implementation. *Chem. Soc. Rev.* 2023, 52, 6294–6329.
- (6) Medina, D. D.; Sick, T.; Bein, T. Photoactive and conducting covalent organic frameworks. *Adv. Energy Mater.* **2017**, *7*, 1700387.
- (7) Kumar, R.; Ansari, S. N.; Deka, R.; Kumar, P.; Saraf, M.; Mobin, S. M. Progress and perspectives on covalent-organic frameworks (COFs) and composites for various energy applications. *Chem. Eur. J.* **2021**, 13669–13698.
- (8) Inácio, D.; Pinto, A. L.; Paninho, A. B.; Branco, L. C.; Freitas, S. K. S.; Cruz, H. Application of covalent organic frameworks (COFs) as dyes and additives for dyesensitized solar cells (DSSCs). *Nanomaterials* 2023, 13, 1204.
- (9) Yang, Y.; Sandra, A. P.; Idström, A.; Schäfer, C.; Andersson, M.; Evenäs, L.; Börjesson, K. Electroactive covalent organic framework enabling photostimulusresponsive devices. J. Am. Chem. Soc. 2022, 144, 16093–16100.
- (10) Martínez-Fernández, M.; Martínez-Periñán, E.; Royuela, S.; Martínez, J. I.; Zamora, F.; Lorenzo, E.; Segura, J. Covalent organic frameworks based on electroactive naph-

- thalenediimide as active electrocatalysts toward oxygen reduction reaction. *Appl. Mater. Today* **2022**, *26*, 101384.
- (11) Liu, S.; Wang, M.; He, Y.; Cheng, Q.; Qian, T.; Yan, C. Covalent organic frameworks towards photocatalytic applications: Design principles, achievements, and opportunities. *Coord. Chem. Rev.* **2023**, *475*, 214882.
- (12) Altinişik, S.; Yanalak, G.; Patir, I.; Koyuncu, S. Viologen-based covalent organic frameworks toward metal-free highly efficient photocatalytic hydrogen evolution. ACS Appl. Mater. Interfaces 2023, 15, 18836–18844.
- (13) Qi, S.; Guo, R.; Bi, Z.; Zhang, Z.; Li, C.; Pan, W. Recent progress of covalent organic frameworks-based materials in photocatalytic applications: A review. *Small* **2023**, *19*, 2303632.
- (14) Wang, M.; Liang, G.; Wang, M.; Hu, M.; Zhu, L.; Li, Z.; Zhang, Z.; He, L.; Du, M. Electroactive and photoactive porphyrin-based covalent-organic framework for the construction of a bifunctional self-powered sensing platform toward real time analysis of nitride oxide from cancer cells. *Chem. Eng. J.* **2022**, *448*, 137779.
- (15) Zhao, R.; Wang, T.; Li, J.; Shi, Y.; Hou, M.; Yang, Y.; Zhang, Z.; Lei, S. Two-dimensional covalent organic frameworks for electrocatalysis: Achievements, challenges, and opportunities. *Nano Res.* 2023, 16, 8570–8595.
- (16) Fan, Y.; Chen, M.; Xu, N.; Wang, K.; Gao, Q.; Liang, J.; Liu, Y. Recent progress on covalent organic framework materials as CO<sub>2</sub> reduction electrocatalysts. Front. Chem. 2022, 10, 942492.
- (17) Li, H.; Wang, L.; Yu, G. Covalent organic frameworks: Design, synthesis, and performance for photocatalytic applications. *Nano Today* **2021**, *40*, 101247.

- (18) Chen, Z.; Wang, J.; Hao, M.; Xie, X., Y. Liu; Yang, H.; Waterhouse, G. I. N.; Wang, X.; Ma, S. Tuning excited state electronic structure and charge transport in covalent organic frameworks for enhanced photocatalytic performance. *Nat. Commun.* 2023, 14, 1106.
- (19) Li, Y.-J.; Cui, W.-R.; Jiang, Q.-Q.; Wu, Q.; Liang, R.-P.; Luo, Q.-X.; Qiu, J.-D. A general design approach toward covalent organic frameworks for highly efficient electrochemiluminescence. *Nat. Commun.* **2021**, *12*, 4735.
- (20) Zhang, L.; Zhang, X.; Han, D.; Zhai, L.; Mi, L. Recent progress in design principles of covalent organic frameworks for rechargeable metal-ion batteries. Small Methods 2023, 7, 2300687.
- (21) Yang, J.; Kang, F.; Wang, X.; Zhang, Q. Design strategies for improving the crystallinity of covalent organic frameworks and conjugated polymers: a review. *Mater. Horiz.* **2022**, *9*, 121–146.
- (22) Li, X.; Gao, Q.; Wang, J.; Chen, Y.; Chen, Z.-H.; Xu, H.-S.; Tang, W.; Leng, K.; Ning, G.-H.; Wu, J. et al. Tuneable near white-emissive two-dimensional covalent organic frameworks. *Nat. Commun.* **2018**, *9*, 2335.
- (23) Deshaye, M.; Pollard, Z. A.; Banducci, A.; Goodey, A.; Prommin, C.; Kanlayakan, N.; Kungwan, N.; Kowalczyk, T. Accessible and efficient modeling of chromophores within time-independent excited-state density functional tight-binding: Concepts and applications. *Physical Chemistry Research at Undergraduate Institutions: Innovative and impactful approaches* **2022**, *2*, 125–144.
- (24) Fernandes, S. P. S.; Frey, L.; Cid-Seara, K. M.; Oliveira, O.; Guldris, N.; Carbó-Argibay, E.; Rodríguez-Abreu, C.; Kolenko, Y. V.; Silva, A. M. S.; Medina, D. D. et al. A post-synthetic modification strategy for the synthesis of pyrene-fused azaacene covalent organic frameworks. *Microporous Mesoporous Mater.* 2022, 343, 112162.

- (25) Wang, C.; Zhang, Z.; Zhu, Y.; Yang, C.; Wu, J.; Hu, W. 2D covalent organic frameworks: From synthetic strategies to advanced optical-electrical-magnetic functionalities. *Adv. Mater.* **2022**, *34*, 2102290.
- (26) Sharma, R. K.; Yadav, P.; Yadav, M.; Gupta, R.; Rana, P.; Srivastava, A.; Zbořil, R.; Varma, R. S.; Antonetti, M.; Gawande, M. B. Recent development of covalent organic frameworks (COFs): synthesis and catalytic (organic-electro-photo) applications. *Mater. Horiz.* 2020, 7, 411–454.
- (27) Li, X.; Cai, S.; Sun, B.; Yang, C.; Zhang, J.; Liu, Y. Chemically robust covalent organic frameworks: Progress and perspective. *Matter* **2020**, *3*, 1507–1540.
- (28) Frey, L.; Oliveira, O.; Sharma, A.; Guntermann, R.; Fernandes, S. P. S.; Cid-Seara, K. M.; Abbay, H.; Thornes, H.; Rocha, J.; Döblinger, M. et al. Building blocks and COFs formed in concert three-component synthesis of pyrene-fused azaacene covalent organic framework in the bulk and as films. *Angew. Chem. Int. Ed* **2023**, *62*, e202302872.
- (29) Lan, Y.; Tong, M.; Yang, Q.; Zhong, C. Computational screening of covalent organic frameworks for the capture of radioactive iodine and methyl iodide. *Cryst. Eng. Comm.* **2017**, *19*, 4920–4926.
- (30) Altundal, O. F.; Altintas, C.; Keskin, S. Can COFs replace MOFs in flue gas separation? High-throughput computational screening of COFs for CO<sub>2</sub>/N<sub>2</sub> separation. *J. Mater. Chem. A* 2020, 8, 14609–14623.
- (31) Feng, M.; Cheng, M.; Deng, J.; Ji, X.; Zhou, L.; Dang, Y.; Bi, K.; Dai, Z.; Dai, Y. High-throughput computational screening of covalent-organic framework membranes for helium purification. *Results Eng.* **2022**, *15*, 100538.
- (32) Aydin, S.; Altintas, C.; Keskin, S. High-throughput screening of COF membranes and

- COF/polymer MMMs for helium separation and hydrogen purification. *ACS Appl. Materl. Interfaces* **2022**, *14*, 21738–21749.
- (33) Mourino, B.; Jablonka, K. M.; Ortega-Guerrero, A.; Smit, B. In search of covalent organic framework photocatalysts: A DFT-based screening approach. *Adv. Funct. Mater.* **2023**, *33*, 2301594.
- (34) Wen, S.-H.; Li, A.; Song, J.; Deng, W.-Q.; Han, K.-L.; Goddard III, W. A. First-principles investigation of anisotropic hole mobilities in organic semiconductors. *J. Phys. Chem. B* **2009**, *113*, 8813–8819.
- (35) Giannini, S.; Blumberger, J. Charge transport in organic semiconductors: The perspective from nonadiabatic molecular dynamics. *Acc. Chem. Res.* **2022**, *55*, 819–930.
- (36) Chu, T.; Liu, Y. A theoretical approach for simulations of anisotropic charge carrier mobility in organic single crystal semiconductors. *Org. Electron.* **2018**, *53*, 165–184.
- (37) Kitoh-Nishioka, H.; Welke, K.; Nishimoto, Y.; Fedorov, D. G.; Irle, S. Multiscale simulations on charge transport in covalent organic frameworks including dynamics of transfer integrals from the FMO-DFTB/LCMO approach. *J. Phys. Chem. C* **2017**, 121, 17712–17726.
- (38) Jin, E.; Geng, K.; Fu, S.; Yang, S.; Kanlayakan, N.; Addicoat, M. A.; Kungwan, N.; Geurs, J.; Xu, H.; Bonn, M. et al. Exceptional electron conduction in two-dimensional covalent organic frameworks. *Chem* **2021**, *7*, 3309–3324.
- (39) Ghosh, S.; Tsutsui, Y.; Kawaguchi, T.; Matsuda, W.; Nagano, S.; Suzuki, K.; Kaji, H.; Seki, S. Band-like transport of charge carriers in oriented two-dimensional conjugated covalent organic frameworks. *Chem. Mater.* **2022**, *34*, 736–745.
- (40) Patwardhan, S.; Kocherzhenko, A. A.; Grozema, F. C.; Siebbeles, L. D. A. Delocaliza-

- tion and mobility of charge carriers in covalent organic frameworks. J. Phys. Chem. C **2011**, 115, 11768–11772.
- (41) Cave, R. J.; Newton, M. D. Generalization of the Mulliken-Hush treatment for the calculation of electron transfer matrix elements. *Chem. Phys. Lett.* **1996**, *249*, 15–19.
- (42) Zheng, J.; Beratan, D. N. Generalized Mulliken-Hush analysis of electronic coupling interactions in compressed π-stacked porphyrin-bridge-quinone systems. J. Am. Chem. Soc. 2005, 127, 11303–11310.
- (43) Subotnik, J. E.; Yeganeh, S.; Cave, R. J.; Ratner, M. A. Constructing diabatic states from adiabatic states: Extending generalized Mulliken-Hush to multiple charge centers with Boys localization. *J. Chem. Phys.* **2008**, *129*, 244101.
- (44) Guo, X.; Qu, Z.; Gao, J. The charge transfer electronic coupling in diabatic perspective: A multi-state density functional theory study. *Chem. Phys. Lett.* **2018**, *691*, 91–97.
- (45) Wu, Q.; Van Voorhis, T. Extracting electron transfer coupling elements from constrained density functional theory. *J. Chem. Phys.* **2006**, *125*, 164105.
- (46) Kaduk, B.; Kowalczyk, T.; Van Voorhis, T. Constrained density functional theory. *Chem. Rev.* **2012**, *112*, 321–370.
- (47) Voityuk, A. A. Electronic couplings for photoinduced electron transfer and excitation energy transfer computed using excited states of noninteracting molecules. *J. Phys. Chem. A* **2017**, *121*, 5414–5419.
- (48) Kohn, J. T.; Gildemeister, N.; Grimme, S.; Fazzi, D.; Hansen, A. Efficient calculation of electronic coupling integrals with the dimer projection method via a density matrix tight-binding potential. *J. Chem. Phys.* **2023**, *159*, 144106.
- (49) Laszlo, V.; Kowalczyk, T. Acene-linked covalent organic frameworks as candidate materials for singlet fission. J. Mater. Chem. A 2016, 4, 10500–10507.

- (50) Dogru, M.; Handloser, M.; Auras, F.; Kunz, T.; Medina, D.; Hartschuh, A.; Knochel, P.; Bein, T. A photoconductive thienothiophene-based covalent organic framework showing charge transfer towards included fullerene. *Angew. Chem. Int. Ed* **2013**, *52*, 2920–2924.
- (51) Frenzel, J.; Oliveira, A. F.; Jardillier, N.; Heine, T.; Seifert, G. Semi-relativistic, self-consistent charge Slater-Koster tables for density-functional based tight-binding (DFTB) for materials science simulations; 2004-2009.
- (52) Lukose, B.; Kuc, A.; Frenzel, J.; Heine, T. On the reticular construction concept of covalent organic frameworks. *J. Nanotechnol.* **2010**, *1*, 60–70.
- (53) Hourahine, B.; Aradi, B.; Blum, V.; Bonafé, F.; Buccheri, A.; Camacho, C.; Cevallos, C.; Deshaye, M. Y.; Dumitrică, T.; Dominguez, A. et al. DFTB+, a software package for efficient approximate density functional theory based atomistic simulations. J. Chem. Phys. 2020, 152, 124101.
- (54) Perdew, J. P.; Burke, K.; Ernzerhof, M. Generalized gradient approximation made simple. *Phys. Rev. Lett.* **1996**, *77*, 3865–3868.
- (55) Becke, A. D. Density-functional Thermochemistry .3. The Role of Exact Exchange. *J. Chem. Phys.* **1993**, *98*, 5648–5652.
- (56) Epifanovsky, E.; Gilbert, A. T. B.; Feng, X.; Lee, J.; Mao, Y.; Mardirossian, N.; Pokhilko, P.; White, A. F.; Coons, M. P.; Dempwolff, A. L. et al. Software for the frontiers of quantum chemistry: An overview of developments in the Q-Chem 5 package. J. Chem. Phys. 2021, 155, 084801.
- (57) Wakayama, Y.; Hayakawa, R.; Chikyow, T.; Machida, S.; Nakayama, T.; Egger, S.; de Oteyza, D. G.; Dosch, H.; Kobayashi, K. Self-assembled molecular nanowires of 6,13-Bis(methylthio)pentacene: Growth, electrical properties, and applications. *Nano Lett.* **2008**, *8*, 3273–3277.

- (58) Wang, M.; Ballabio, M.; Wang, M.; Lin, H.-H.; Biswal, B. P.; Han, X.; Paasch, S.; Brunner, E.; Liu, P.; Chen, M. et al. Unveiling electronic properties in metal-phthalocyanine-based pyrazine-linked conjugated two-dimensional covalent organic frameworks. *J. Am. Chem. Soc.* **2019**, *141*, 16810–16816.
- (59) Smith, M. B.; Michl, J. Singlet Fission. Chem. Rev. 2010, 110, 6891–6936.
- (60) Greyson, E. C.; Stepp, B. R.; Chen, X.; Schwerin, A. F.; Paci, I.; Smith, M. B.; Akdag, A.; Johnson, J. C.; Nozik, A. J.; Michl, J. et al. Singlet exciton fission for solar cell applications: Energy aspects of interchromophore coupling. J. Phys. Chem. B 2010, 114, 14223–14232.
- (61) Saegusa, T.; Sakai, H.; Nagashima, H.; Kobori, Y.; Tkachenko, N. V.; Hasobe, T. Controlled orientations of neighboring tetracene units by mixed self-assembled monolayers on gold nanoclusters for high-yield and long-lived triplet excited states through singlet fission. J. Am. Chem. Soc. 2019, 141, 14720–14727.
- (62) Wu, X.; Han, X.; Liu, Y.; Liu, Y.; Cui, Y. Control interlayer stacking and chemical stability of two-dimensional covalent organic frameworks via steric tuning. J. Am. Chem. Soc. 2018, 140, 16124–16133.
- (63) Wang, Z.; Zhang, Y.; Wang, T.; Lin, E.; Wang, T.; Chen, Y.; Cheng, P.; Zhang, Z. Modulating the interlayer stacking of covalent organic frameworks for efficient acetylene separation. *Small* **2023**, *19*, 2303684.
- (64) Liu, M.; Fu, Y.; Bi, S.; Yang, S.; Yang, X.; Li, X.; Chen, G. J.; He, J.; Xu, Q.; Zeng, G. Dimensionally-controlled interlayer spaces of covalent organic frameworks for the oxygen evolution reaction. *Chem. Eng. J.* 2024, 479, 147682.
- (65) Calik, M.; Auras, F.; Salonen, L. M.; Bader, K.; Grill, I.; Handloser, M.; Medina, D. D.; Dogru, M.; Löbermann, F.; Trauner, D. et al. Extraction of photogenerated electrons

- and holes from a covalent organic framework integrated heterojunction. *J. Am. Chem. Soc.* **2014**, *136*, 17802–17807.
- (66) Streater, D. H.; Kennehan, E. R.; Wang, D.; Fiankor, C.; Chen, L.; Yang, C.; Li, B.; Liu, D.; Ibrahim, F.; Hermans, I. et al. Control over charge separation by imine structural isomerization in covalent organic frameworks with implications on CO<sub>2</sub> photoreduction. J. Am. Chem. Soc. 2024, 146, 4489–4499.
- (67) Fukuzumi, S.; Itoh, A.; Suenobu, T.; Ohkubo, K. Formation of the Long-Lived Charge-Separated State of the 9-Mesityl-10-methylacridinium Cation Incorporated into Mesoporous Aluminosilicate at High Temperatures. J. Phys. Chem. C 2014, 118, 24188–24196.
- (68) Garcia, N.; Kowalczyk, T. Extension of intramolecular charge-transfer state lifetime by encapsulation in porous frameworks. *J. Phys. Chem. C* **2017**, *121*, 20673–20679.
- (69) Kim, H.; Goodson III, T.; Zimmerman, P. M. Density functional physicality in electronic coupling estimation: Benchmarks and error analysis. J. Phys. Chem. Lett. 2017, 8, 3242–3248.
- (70) Dontot, L.; Suaud, N.; Rapacioli, M.; Spiegelman, F. An extended DFTB-CI model for charge-transfer excited states in cationic molecular clusters: model studies versus ab initio calculations in small PAH clusters. *Phys. Chem. Chem. Phys.* 2016, 18, 3545– 3557.
- (71) Croy, A.; Unsal, E.; Biele, R.; Pecchia, A. DFTBephy: A DFTB-based approach for electron-phonon coupling calculations. *J. Comput. Electron.* **2023**, *22*, 1231–1239.